JACS
JOURNAL OF THE AMERICAN CHEMICAL SOCIETY
pubs.acs.org/JACS
Article

Spin Delocalization, Polarization, and London Dispersion Forces Govern the Formation of Diradical Pimers

Joshua P. Peterson, Arkady Ellern, and Arthur H. Winter*

Cite This: J. Am. Chem. Soc. 2020, 142, 5304−5313
Read Online
ACCESS | Metrics & More | Article Recommendations | Supporting Information

ABSTRACT: Some free radicals are stable enough to be isolated, but most are either unstable transient species or exist as metastable species in equilibrium with a dimeric form, usually a spin-paired sigma dimer or a pi dimer (pimer). To gain insight into the different modes of dimerization, we synthesized and evaluated a library of 15 aryl dicyanomethyl radicals in order to probe what structural and molecular parameters lead to σ- versus π-dimerization. We evaluated the divergent dimerization behavior by measuring the strength of each radical association by variable-temperature electron paramagnetic resonance spectroscopy, determining the mode of dimerization (σ- or π-dimer) by UV−vis spectroscopy and X-ray crystallography, and performing computational analysis. We evaluated three different hypotheses to explain the difference in the dimerization behavior: (1) that the dimerization behavior is dictated by radical spin densities; (2) that it is dictated by radical polarizability; (3) that it is dictated by London dispersion stabilization of the pimer. However, no single parameter model in itself was predictive. Two-parameter models incorporating either the computed degree of spin delocalization or the radical polarizability as well as computed estimates for the attractive London dispersion forces in the π-dimers lead to improved forecasts of σ- vs π-dimerization mode, and suggest that a balance of spin delocalization of the isolated radical as well as attractive forces between the stacked radicals, govern the formation of diradical pimers.

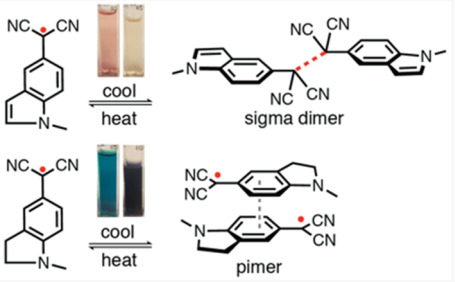

INTRODUCTION

Free radicals pervade all aspects of chemistry, from synthetic mechanisms to materials science to biological chemistry. Some free radicals can be stabilized sufficiently to make them isolable. Just below this point of indefinite persistence are metastable radicals that exist in a dynamic equilibrium with dimers. An example of such a metastable radical is the trityl radical, the first detected free radical, which famously exists in a solution-phase equilibrium with a head-to-tail σ-dimer.[1] This radical dimerization can be an annoyance when attempting to make ferromagnetic plastics, but is an attractive feature when using these radicals as building blocks for stimuli responsive materials, dynamic covalent assemblies, chemical sensors with optical or magnetic resonance contrast, or organic spin-crossover materials.[2−10]

A wealth of literature on such metastable radical species shows that they form either weak σ-dimers or multicentered π-dimers (pimers).[11,12] The radical—radical bond found in these pimers is fascinating for its unusual multicenter covalent bonding pattern that brings the atoms closer than the van der Waals radii but much longer than a conventional two-atom bond (>2.8 Å), while straddling the knife edge between van der Waals interactions and conventional chemical bonds in strength and properties. Unfortunately, models to understand why some metastable radicals form σ-dimers while others form pimers are lacking.

Understanding this divergent dimerization behavior would aid in the application of these radicals into useful materials, because the properties of the two types of radical dimers show remarkable differences. For example, σ-dimers usually absorb mostly in the UV region of the optical spectrum and have properties that are more consistent with "normal" closed-shell organic molecules. In contrast, diradical pimers are typically colored species that absorb visible to near-infrared light and feature unusual conductive and magnetic properties.[18,22,23] Such radical pimers, or "pancake dimers",[21] are distinct from normal pi-stacked dimers between closed-shell aromatics because they often prefer face-to-face sandwich geometries rather than slip-stacked geometries. Moreover, unlike normal π-stacked dimers, they can have strong orientational geometric preferences, are stabilized by π orbital interactions (rather than being repulsive), have fluxional geometries, and often show large intramolecular and layer-to-layer charge transporting properties with broader energy bands than typical organic semiconductors.

Select examples of metastable radicals are shown in Figure 1, along with their preferred mode of dimerization. For example, phenalenyl radicals and triangulene radicals can form either σ-

Received: January 7, 2020
Published: February 22, 2020

https://dx.doi.org/10.1021/jacs.0c00190
J. Am. Chem. Soc. 2020, 142, 5304−5313

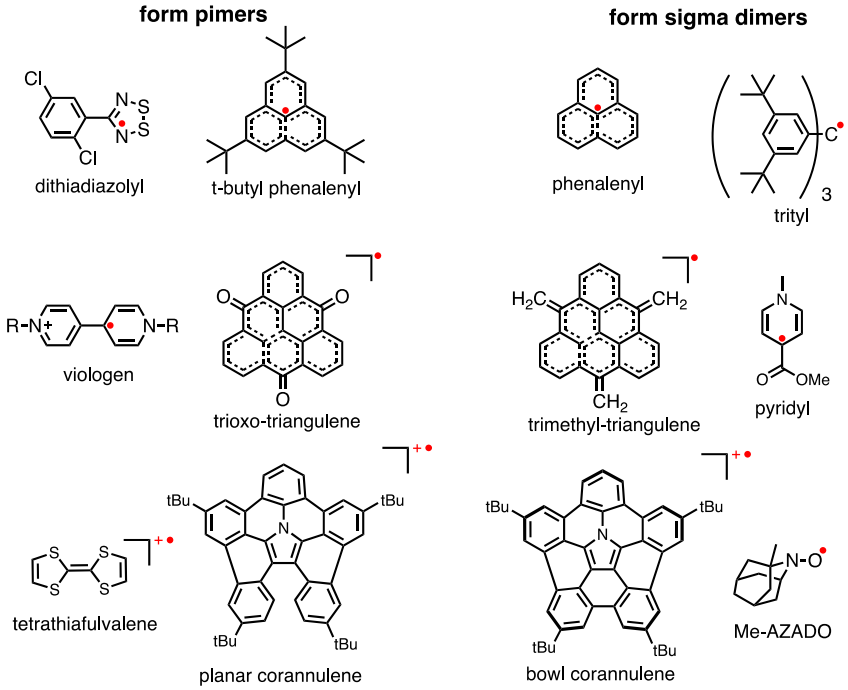

Figure 1. Examples of radicals that form sigma[13−17] and π-dimers.[16,18−21]

or π-dimers depending on the substitution.[20,24−26] Examples of radicals that form σ-dimers include trityl radicals,[13,14] pyridyl radicals,[27] and aza-adamantyl nitroxyl radicals.[17] Radicals that form pimers include halo-phenyl dithiazolyl radicals,[19] planar corranulene-derived cation radicals,[16] viologen cation radicals,[18] π-radical anions such as tetracyanoquinodimethane (TCNQ),[11] and naphthalene diimide radical anions,[12] although many others are known.[28−30]

To understand what structural and molecular parameters dictate whether a σ- or π-dimer is formed for that radical, a library of aryl dicyanomethyl radicals was synthesized and evaluated. As shown by Seki and co-workers,[32−34] and subsequently by us,[31,35−37] this class of radicals are indefinitely stable provided a *para* substituent is added to block an irreversible head-to-tail dimerization reaction. They exist as stable steady state populations of radical in equilibrium with dimers. These radicals are attractive for such a study because they are known to dimerize to form either a σ-dimer or a pimer depending on the attached substituents. For example, a *p*-dimethylamino derivative forms a σ-dimer, while a structurally related julolidine derivative forms a pimer, with no obvious explanation for the difference (see Figure 2).

To elucidate the structural and molecular parameters that direct the formation of σ- and π-dimerization, a library of radicals was investigated using variable temperature electron paramagnetic resonance (EPR) spectroscopy, variable temperature (VT)-UV−vis spectroscopy, X-ray crystallography, and computational analysis. The synthesized library is shown in Figure 4, and it explores the structural region around these two known radicals (**6**, **15**) featuring different dimerization modes. We evaluated three competing hypotheses—one based on spin delocalization, one based on radical polarizability, and one based on London dispersion forces—to explain the divergent modes of dimerization, with the hopes of developing a predictive model that could be used to both explain the modes of dimerization for known radicals and ideally allow forecasts of the dimerization mode for novel radicals (Figure 3), and

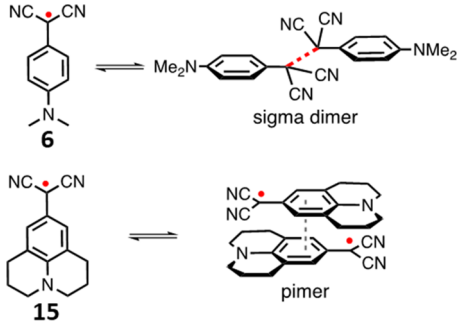

Figure 2. Known modes of dimerization for the dimethylamino[31] and julolidine[32] substituted dicyanomethyl radicals.

provide fundamental insight into the important properties driving the formation of the two different types of dimers.

This investigation reveals that radical spin delocalization is a key parameter for predicting σ- or π-dimerization. For example, all radicals in this work with highly localized spin densities form σ-dimers. However, with delocalized spin densities, either π-dimers or σ-dimers can form. Within this regime, spin delocalization is an insufficiently predictive parameter in isolation. A two-parameter model incorporating either the computed spin density or the radical polarizability and a computational estimate of the dispersion forces in the stacked pimers leads to improved two-parameter models for predicting the mode of dimerization and suggests that both spin delocalization and attractive forces between the stacked radicals are critical to understanding the dimerization mode of metastable radicals.

RESULTS AND DISCUSSION

Structural Effects on the Radical-Dimer Equilibrium Constants. A library of aryl dicyanomethyl radicals with *para* substituted electron donating groups were prepared by oxidation of the precursor aryl malononitriles by previously

https://dx.doi.org/10.1021/jacs.0c00190
J. Am. Chem. Soc. 2020, 142, 5304−5313

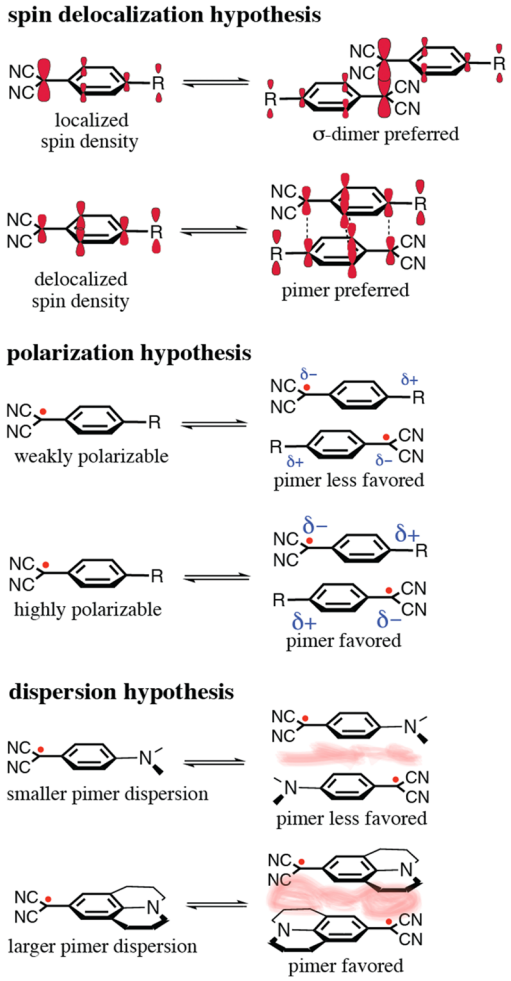

Figure 3. Schematic of spin delocalization hypothesis for maximizing covalent bonding, polarization hypothesis for maximizing Coulombic interactions, and dispersion hypothesis for maximizing London dispersion forces.

reported experimental methods[31,32] (Figure 4). The library was made to span the structural space between radicals **6** and **15** (Figure 2). All synthetic procedures are provided in the Supporting Information.

In order to decouple steric effects of the substituents, with the exception of **3**, substituents were appended to the *meta* and *para* positions relative to the radical center. Consequently, these substituents are anticipated to have little steric effect on the stability of the σ-dimer (see Figure 4 for crystal structures of some of the dimers). Eleven of the 15 radicals in Figure 4 are new structures, while four of them have been previously reported either by us (**1**, **3**, and **6**)[31] or Seki and co-workers (**15**).[32] Radical association constants for dimerization were determined from van 't Hoff plots obtained by determining the radical/dimer equilibrium constants at varying temperatures using variable-temperature EPR spectroscopy (Table 1 shows an example van 't Hoff plot; all van 't Hoff plots are shown in the Supporting Information).

As can be seen in Table 1, the electronic donating ability of the *para* substituent is inversely correlated with the dimerization association constant. Thus, radicals with strong donating groups are stabilized and feature lower K_a values for dimerization than radicals substituted with less strong donors. With less strongly electron donating substituents, such as oxo-substitution in the *para* position, K_a values between 10^5 and 10^6 M^{-1} were obtained irrespective of whether the substituent was freely rotating (radicals **1**−**3**) or locked in a fused ring (radicals **4** and **5**). These radicals form σ-dimers as shown by variable temperature UV−vis experiments described later and by crystal structures determined for **3** and **4** (see Figure 4). For all radicals that form σ-dimers, at low temperature, the solution is clear or yellow and becomes brightly colored upon heating as the colored radical is liberated.

In contrast, *para* amino substituents stabilize the radical by orders of magnitude compared to oxo-substituents.[31,36] Radicals **6**−**14** are examples of radicals that feature a *para* amino substituent, with **6**−**8** having free substituent rotation while **9**−**14** are constrained by a ring that both hinders free rotation and nitrogen pyramidalization. Hindering pyramidalization of the amino substituent certainly favors more delocalization into the aromatic ring by maximizing p character without the usual energetic penalty for rehybridization at nitrogen.[38,39] For radicals **6**−**8** and **11**−**14**, association constants for these radicals range from 10^2−10^4 M^{-1}. Thus, in contrast to radicals with oxo substituents, at room temperature a large fraction of the sample exists as the free radical rather than the dimer and the solutions are highly colored even at room temperature (at millimolar or lower concentrations). Radicals **9** and **10**, indole derivatives, are exceptional cases and feature larger association constants, more

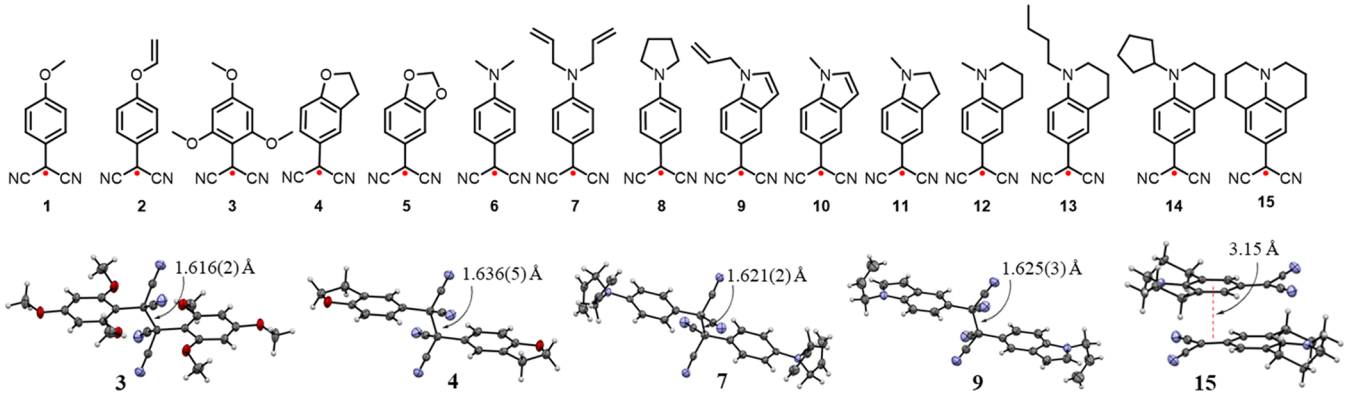

Figure 4. Radicals studied here with crystal structures of the radical dimers (crystal structures for **3** and **15** are reproduced from prior work,[31,32] while crystals of **4**, **7**, and **9** were crystallized from chloroform and their structures are new to this study). Radicals **1**, **3**, **6**, and **15** were previously reported,[31,32] while the other 11 radicals are new to this study.

https://dx.doi.org/10.1021/jacs.0c00190
J. Am. Chem. Soc. 2020, 142, 5304−5313

Table 1. Thermodynamic Data Obtained through VT-EPR, and Computed Mulliken Benzylic Spin Densities (ωB97XD/6-31+G (d,p)) and Estimates of the Relative Pimer Dispersion Energy (Defined As the Sigma Dimer−Pimer Energy Difference Computed at B98 vs B97D, Relative to Radical 2)

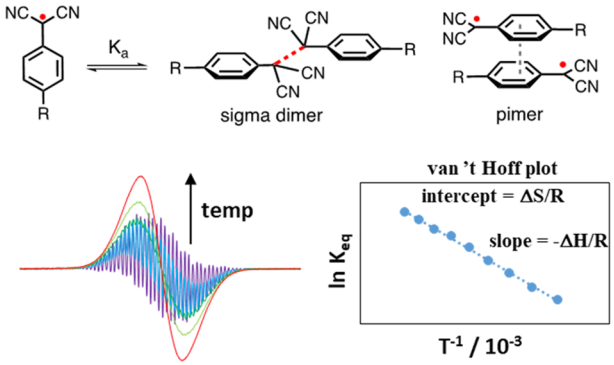

radical	K_a (M^{-1})	solvent	benzylic spin density	relative pimer dispersion	$\Delta G_{dim,298K}$ [kJ mol^{-1}]
1	4.5×10^6	toluene	0.57	NA	−38
2	3.7×10^6	toluene	0.59	0	−38
3	1.9×10^5	toluene	0.56	NA	−30
4	3.5×10^5	toluene	0.54	1.78	−32
5	2.3×10^6	toluene	0.57	1.03	−36
6	2.0×10^5	toluene	0.47	2.49	−29
7	1.7×10^4	toluene	0.49	5.47	−24
8	6.2×10^3	toluene	0.46	2.94	−22
9	1.3×10^5	toluene	0.57	2.95	−35
10	7.0×10^6	toluene	0.57	2.52	−39
11	3.4×10^2	$CHCl_3$	0.45	3.14	−15
12	2.9×10^3	$CHCl_3$	0.44	6.20	−20
13	7.0×10^2	$CHCl_3$	0.44	6.20	−16
14	9.3×10^2	$CHCl_3$	0.44	9.04	−17
15	1.4×10^3	NA	0.40	9.17	−18

similar to those of the oxo-substituted dicyanomethyl radical ($K_a \sim 10^6$ M^{-1}) than typical amino substituents. In these cases, the *para* nitrogen in the indole ring is no longer as strong a donor as a typical amino substituent due to lost electron donation into the aromatic indole ring. These radicals are discussed in more detail below.

Predictive Power and Failures of the Spin Delocalization Hypothesis. A parameter potentially important for directing the mode of radical dimerization is radical spin delocalization. The hypothesis is that radicals with highly localized spins on the benzylic carbon have a greater likelihood for making a σ-dimer because orbital overlap would be maximized in making the two-atom bond (Figure 3, top). However, as the radical becomes more delocalized, the σ bond should get weaker due to diminished overlap. Eventually, in radicals where the spin density becomes highly delocalized, there may come a tipping point where forming a multicentered pimer becomes energetically preferred, where the sum of many weaker π−π stacked SOMO orbital interactions (plus other attractive noncovalent forces and entropic effects) exceeds that of forming one more strongly overlapping two-atom σ-dimer. This hypothesis is related to one suggested by Passmore, White, and co-workers[40] who suggested that there is an energetic penalty for making σ-dimers with highly delocalized radicals, which they used to explain the pimerization of sulfur-containing radicals[40] Consistent with this notion, the recently prepared more localized phosphorus analogs form σ-dimers.[41]

To test this hypothesis, we computed the Mulliken spin densities for each of the radicals in Figure 4 and determined whether the radical forms a σ-dimer or a pimer in solution. Fortunately, it is simple to determine whether the radical makes a σ-dimer or a pimer, because cooling solutions of the colored radical leads to the dimerized form, as shown by a loss of the EPR signal for the radical upon cooling. If the radical forms a σ-dimer, the solution turns clear or yellow upon cooling because the σ-dimer disrupts the π conjugation. The σ-dimer has absorptions mostly in the UV region of the optical spectrum. In contrast, if the radical forms a pimer, the solution becomes more darkly colored than the free radical, as the pimers typically have slightly increased absorptions in the visible region of the optical spectrum. Additionally, the pimers show growth of a new band in the near-IR region of the optical spectrum ∼ 850−900 nm. An example of the difference between a radical forming a σ-dimer and a radical forming a pimer is shown in Figure 5. Time-dependent density functional

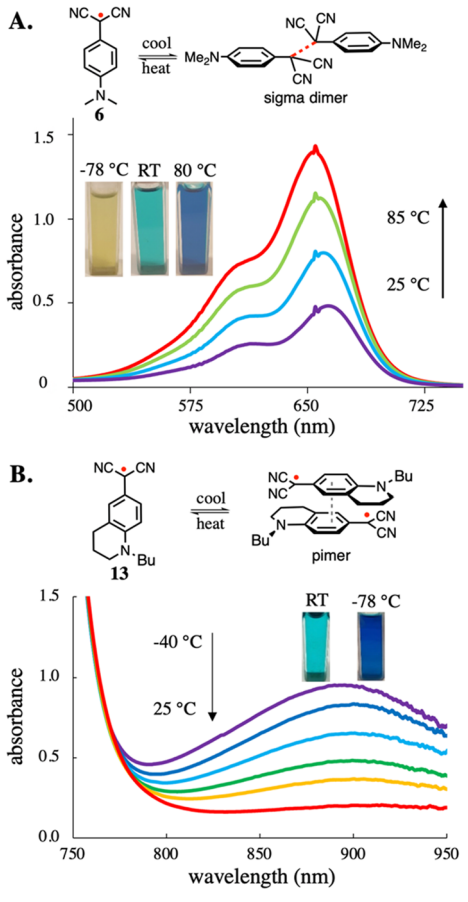

Figure 5. UV−vis of **6** showing σ-dimerization (a). Low temperature UV−vis of **13** showing pimerization (b).

theory (TD-DFT) computations of the UV−vis spectra of the pimers match well with the experimentally determined spectra (see Figure S3 in the Supporting Information).

In all cases, the mode of dimerization in solution matches the mode of dimerization observed in the crystal structure. Radicals **3**, **4**, **7**, and **9** form σ-dimers in the crystal, and these radicals were found to also form σ-dimers in solution. The most noteworthy features of the solid state structures is that

https://dx.doi.org/10.1021/jacs.0c00190
J. Am. Chem. Soc. 2020, 142, 5304−5313

the σ-dimers feature elongated C−C single bonds (>1.6 Å) and adopt an anti conformation. In the case where a crystal structure of a pimer was obtained by Seki and co-workers (**15**),[32] this radical also forms a pimer in solution.

To evaluate whether there is a correlation between the spin density and the radical dimerization mode, we plotted the computed benzylic spin density for each of the radicals versus the experimentally determined association constants for radical dimerization (Figure 6, top). Radicals that were observed to form σ-dimers when the solutions were cooled are depicted as blue triangles while those that were observed to form pimers are depicted with red circles.

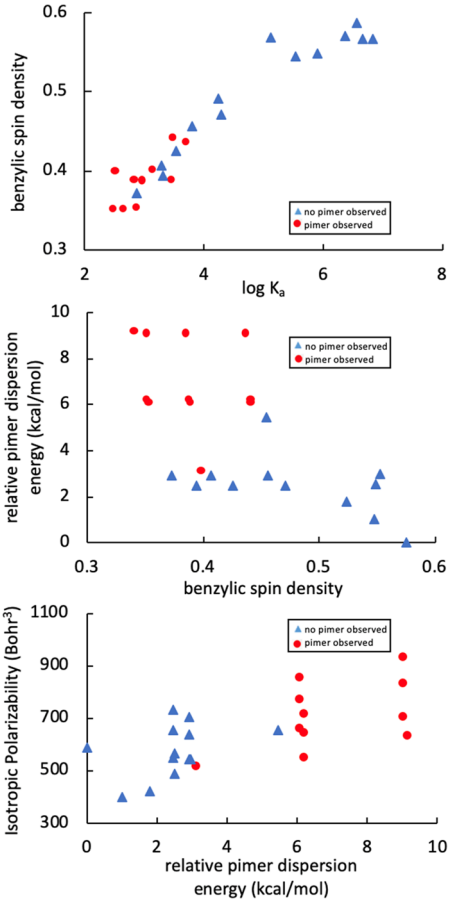

Figure 6. Plot of the log of binding constant vs computed benzylic carbon spin density (top) and a plot of benzylic carbon spin density vs normalized dispersion stabilization energy (middle). In both graphs, red circles signify observed π-dimers and blue triangles represent observed σ-dimers. Versions of these plots with radical labels can be found in Figure SI4.

As can be seen from Figure 6, there is a strong direct correlation between the K_a and the computed spin density on the benzylic carbon. Thus, radicals with large spin densities on the benzylic carbon form stronger bonds. Furthermore, all the aryl dicyanomethyl radicals in this work with a high spin density on the benzylic carbon (>45%) formed σ-dimers, in line with the spin delocalization hypothesis. Also consistent with the hypothesis, all radicals that formed pimers had <45% computed spin density on the benzylic carbon.

However, a number of radicals with <45% spin density also formed σ-dimers. Thus, while the spin delocalization hypothesis shown in Figure 5 explains many of our observations, it cannot, on its own, explain all of the observed radical behavior. Within the regime of radicals having highly delocalized spin densities, it fails to be predictive.

Effect of Pimer Dispersion Stabilization Energy: Incorporation into Two-Parameter Predictive Models. As noted above, the spin delocalization hypothesis fails to be predictive for radicals that feature highly delocalized spins. Thus, we considered that other effects other than spin delocalization may be playing a role in directing the relative energetics of the σ-dimer and pimer. It is known that a variety of pimers such as TCNQ and TCNE radical anions as well as viologen cation radical pimers are stabilized by dispersion forces,[11,12,18] so we considered that perhaps some radicals stack better in the pimers than others, leading to larger stabilizing dispersion energies. We hypothesized that differences in these dispersion forces could explain the differing mode of dimerization for radicals that have similar spin delocalization.

To computationally estimate the dispersion stabilization, we computed the relative energy of the π-dimer and σ-dimer for each radical with two different density functionals, one including a dispersion correction (B97D), and the other without a dispersion correction (B98). The difference in energies gives a "dispersion energy" parameter of the pimer relative to the σ-dimer. These absolute dispersion energies were converted to relative dispersion energies by subtracting the dispersion energy for radical **2**, which had the lowest computed pimer dispersion energy value. Thus, radical **2** has a "relative pimer dispersion" of zero.

A single-parameter model using just the relative pimer dispersion energies (shown in Figure S5) to predict the mode of radical dimzerion is imperfect because, while in general radicals that form pimers have large computed pimer dispersion energies, it is not always true. For example, radical **11** has a small computed pimer dispersion, but forms a pimer in solution. However, when these relative pimer dispersion energies were plotted against the computed spin density to give the two-parameter model shown in Figure 6 (middle), this new two-parameter model is significantly improved compared to the model containing just the spin delocalization parameter (Figure 6, top) or just the pimer dispersion energy (Figure S5). All radicals with experimentally observed π-dimers were all computed to have a relative dispersion stabilization energy greater than 6 kcal/mol, with radical **11** being an exception. Radical **11** has a low pimer dispersion energy but compensates by having sufficient spin delocalization to make the pimer preferred. Intuitively, this result makes sense because radical **11** has a smaller substituent and so would not be expected to have as large a pimer dispersion energy. Yet, having the nitrogen locked into a small ring should make the substituent a very strong donor and lead to larger spin delocalization, favoring the pimer.

Despite some regions of ambiguity at the interface, in general radicals featuring low benzylic spin density and large dispersion energies form pimers, while radicals with high benzylic spin density and low pimer dispersion energies form σ-dimers. This two-parameter model, while imperfect, is clearly an improvement over the model including just the spin density (Figure 6, top), which is nonpredictive in the regime of radicals having low computed benzylic spin density.

Importance of Radical Polarizability: Effect on Pimer Geometries and Energies. We also considered that the polarizability of the radical could play a role in stabilizing the

https://dx.doi.org/10.1021/jacs.0c00190
J. Am. Chem. Soc. 2020, 142, 5304−5313

pimer (hypothesis 2 in Figure 3). If the radical is highly polarizable, it should be able to delocalize its electron density in response to a neighboring electric field, such as a polar solvent or another radical, and potentially allow for attractive electrostatic interactions in the π-dimer. Additionally, donor-substituted radical pimers may also be stabilized by 3e$^-$ radical stabilization (lone pair with radical[39]).

To test this hypothesis, we computed the isotropic radical polarizability for each radical, and also examined the computed charge populations of the free radical relative to the pimer. For weakly polarizable radicals, such as **2** shown in Figure 4, relatively small changes in the charge distribution are observed between the free radical and the pimer. With highly polarizable radicals, such as julolidine-derivative **15**, large changes in the computed Mulliken atomic charges are observed between the free radical and the pimer. For example, the nitrogen and the two adjacent carbons become more positive by 0.78 charge units, while the dicyanomethyl group becomes more negative by 0.30 charge units upon going from the free radical to the pimer.

Two parameter models including the computed radical isotropic polarizability versus the relative pimer dispersion energy is shown in Figure 6 (bottom). This two-parameter model is better than the model containing just the spin delocalization parameter, but radical **11** is a major outlier. As noted above, this radical has a low computed pimer dispersion energy but is observed to form a pimer. For this radical, the two-parameter model fails.

While this two-parameter radical polarizability/pimer dispersion model is insufficient in some cases, this polarization effect explains the observed head-to-tail geometry seen in the crystal structure of pimer **15**. Our attempts to optimize the geometry of head-to-head pimers failed, as these geometries optimized to the gauche σ-dimer minimum, suggesting that the head-to-head pimer may not be even a minimum on the potential energy surface. Intuitively, this result makes sense when considering that a perfect sandwich-stacked pimer would feature repulsive electrostatic interactions, which become favorable in the head-to-tail pimer (see Figure 7A).

It should be noted that the radical spin delocalization, polarizability, and pimer dispersion energies are not decoupled parameters. Radicals that are highly delocalized off of the benzylic carbon are also highly polarizable. This interconnectedness of these parameters can be clearly observed from a plot of the benzylic spin density versus the computed radical polarizability (see Figure S5) and by the solvent-dependence of the computed spin densities of the radicals. For highly polarizable radicals, the spins become more delocalized off of the benzylic carbon and onto the donating *para* substituent as the solvent dielectric increases (see Figure 7 for an example of the spin density plotted against the solvent dielectric with a highly polarizable and less polarizable radical). With weakly polarizable radicals, the spin densities are more localized and do not change significantly as a function of solvent dielectric. This polarizability can be explained by solvent screening of the charge-separated resonance structures that are unique to captodative radicals (Figure 7B). Thus, the spin delocalization parameter "encodes" within it information about the radical polarizability. This feature explains why the two-parameter model containing just the delocalization and dispersion parameters can be successful even though it ignores the effect of radical polarizability, because the polarizability is partially integrated into the spin delocalization parameter.

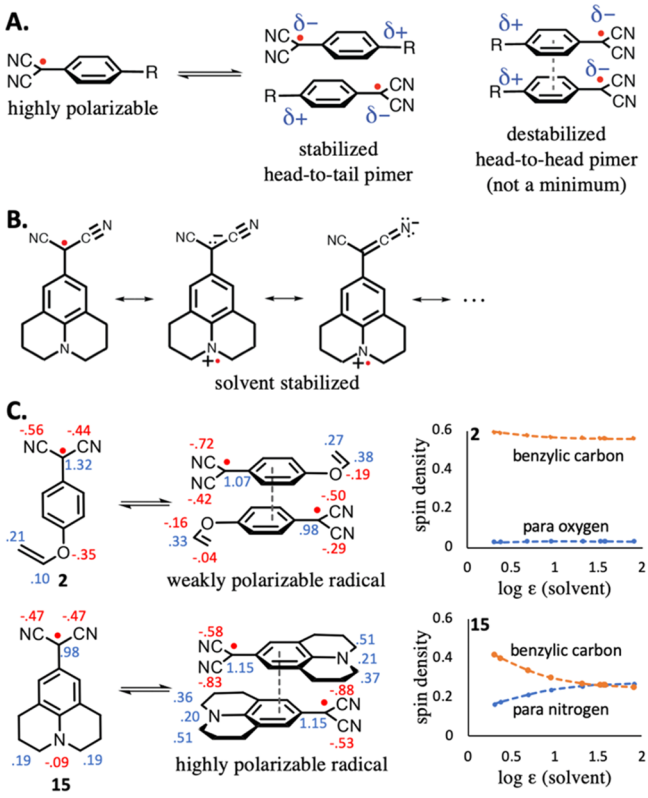

Figure 7. (A) Effect of radical polarization on pimer geometry. (B) Resonance model showing stabilization of polarizable captodative radicals by polar solvents (or the presence of another polarizable radical). (C) Mulliken charge distributions of the pimers of a weakly polarizable radical **2** and a highly polarizable radical **15**. Insets show the computed Mulliken spin densities for the free radical as a function of solvent dielectric (SMD), with increasing contributions of zwitterionic resonance structures in polar solvents for highly polarizable radicals, which lead to diminished benzylic spin density.

The other parameter, the pimer dispersion energy, should also be dependent on both the geometry of the pimer and the polarizability of the two interacting species, with more highly polarizable species leading to higher dispersion energies. Yet, in a practical sense, the computed dispersion energy does not really account for the polarizability of the radical itself. This is because the dispersion corrections included in this B97D functional are akin to a patched-on summation of all the attractive pairwise $1/r^6$ terms in a Lennard–Jones potential added to the DFT energy, with an atom-dependent parametrized coefficient and a damping function to prevent singularities at small r values.[46] This coefficient includes the static dipolar polarizability of the atom, but it is ignorant of the electronic polarizability of the atom in the radical itself. The coefficient will be poorly chosen if the polarizability of the atom in the molecular environment is much different than for the isolated atom, from which the coefficients were obtained. It would not be surprising if atoms in molecular free radicals had different polarizabilities than those for the isolated atoms, as free radicals are expected to be more polarizable than closed-shell species as a general rule. Thus, the dispersion estimates obtained from our DFT model are in reality more decoupled from the polarizability for the predictive model then they would be if more accurate dispersion energies were available.

However, none of our models are successful without including this term, which is the only parameter that has a

https://dx.doi.org/10.1021/jacs.0c00190
J. Am. Chem. Soc. 2020, 142, 5304−5313

dependence on the geometry of the pimer. The polarizability and spin delocalization terms are obtained from computations of the isolated free radicals. Thus, as improvements are made to DFT dispersion corrections to take into account the specifics of the molecular electronic environment, which could be as simple as adjusting the atom-dependent parametrized coefficients, it may be the case that models incorporating the computed dispersion energy will also improve.

Spin Delocalization Effects: What a Difference a Double Bond Makes! From the two-parameter models shown in Figure 6, the pimer dispersion energy appears to be an important parameter in dictating the preferred mode of radical dimerization. We asked the question of whether spin delocalization or dispersion effects were more important in determining the preferred dimerization mode. To answer this question, radicals **10** and **11** were evaluated (Figure 8). These

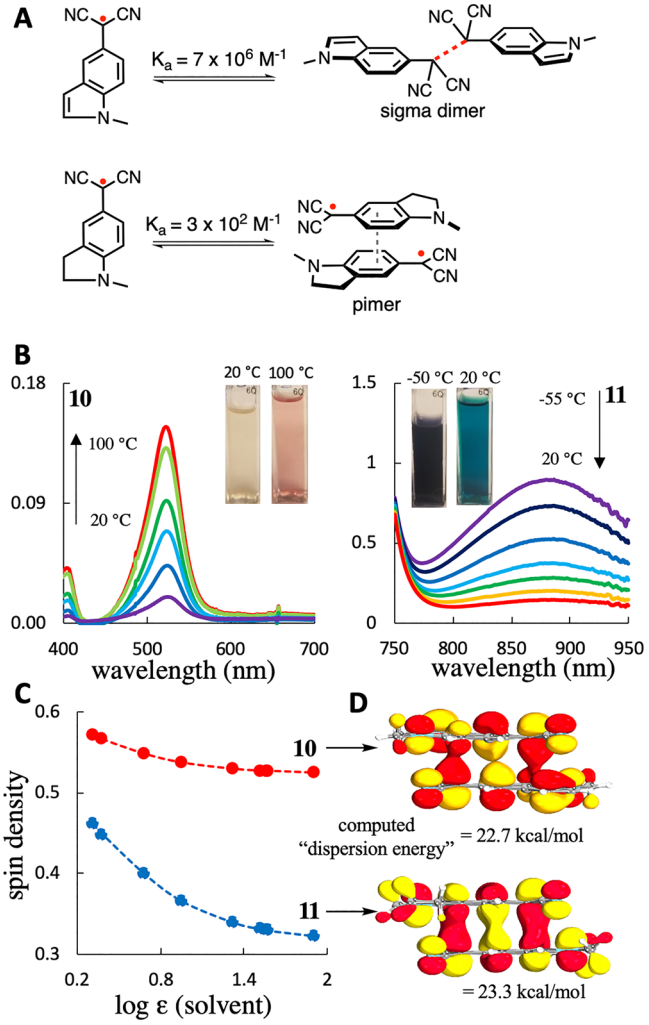

Figure 8. Dimerization of compounds **10** and **11** (a), UV−vis spectra of compounds **10** and **11** (b), and benzylic carbon spin density plot and visualized HOMO (IboView)[42,43] for compounds **10** and **11** (c).

radicals are identical except **10** has an extra double bond. Not surprisingly, then, the computed dispersion energies for the pimers are essentially identical (within 0.6 kcal/mol). Yet, because the indole radical **10** has its lone pair tied into an aromatic ring, it is a *much* weaker donor than **11**. For example, the computed benzylic carbon spin densities (see Figure 8C) for **10** range from 57 to 52% (indicating it is weakly polarizable) while **11** spans the range of 46−32% (indicating it is highly polarizable), depending on the solvent polarity. We anticipated that if dispersion forces directed pimer formation, then both **10** and **11** might form pimers. If spin delocalization was a more important parameter, than **11** might form a pimer, while **10** would not.

The latter outcome proves to be the case. We observe that **10** forms a σ-dimer while **11** forms a pimer (see Figure 8). Indeed, **10** has the largest association constant of all the radicals we tested ($\sim 7 \times 10^6$ M^{-1}) while **11** has the smallest value (3×10^2 M^{-1}) of all radicals tested—a factor of greater than 4 orders of magnitude difference in radical stability! UV−vis spectroscopy (Figure 8B) shows that **10** exists mostly as a σ-dimer at room temperature and upon heating liberates the free radical with a λ_{max} = 525 nm ($K_d \sim 1 \times 10^{-7}$ M). Conversely, **11** exists as a significant portion of radical at room temperature evidenced by large radical band between 600 and 700 nm ($K_d \sim 3 \times 10^{-3}$ M). When cooled, radical **11** shows a pimer band grow in ∼880 nm (Figure 8B) and shows no decrease in the visible region absorption. Visually, the two radicals have "radically" different behavior, with **10** appearing slightly yellow at room temperature (mostly σ-dimer) and becoming pink as the free radical is liberated at high temperature. In contrast, **11** is blue at room temperature as a result of a large thermal population of free radical and becomes a darker blue upon cooling as the pimer forms. Given that the pimer dispersion energy is computed to be essentially identical for these radicals, but these radicals have drastically different spin delocalization/polarization, we conclude that dispersion effects in the pimer cannot be exclusively the driving force for pimerization, and are perhaps subordinate to the electronic substituent effects that lead to spin delocalization/polarization.

COMPUTATIONAL METHODS

To compute spin density and polarizabilities for each radical, geometries were optimized at the ωB97XD[44]/6-31+G(d,p) level of theory using Gaussian16[45] using the SMD solvation model. Previous work had determined this functional and basis set accurate for obtaining the free radical/σ dimer equilibrium thermodynamic values for dicyanomethyl radicals.[37] Mulliken spin densities were used to determine how the spin density varied with solvent for different radicals. For the computation of the π-dimer dispersion stabilization energy, all radicals were optimized at both their σ-dimer and π-dimer geometries at the ωB97XD/6-31+G(d,p) level of theory and then a single-point energy computation was conducted using both B97D[46]/6-31+G(d,p) and B98[47]/6-31+G(d,p) for the π-dimer and σ-dimer. The difference in the σ-dimer/pimer equilibrium ΔE values between the two functionals were given relative to radical **2** to give the "relative pimer dispersion energy" parameter. Radical **2** had the lowest computed pimer dispersion energy so it was defined as zero. It should be noted that the pimers are unstable with respect to an RHF-UHF perturbation. Thus, we also optimized the pimers using a broken-symmetry unrestricted singlet approach to allow for singlet diradical character and calculated the "dispersion energies" at those new geometries. An alternative plot for Figure 6 (pimer dispersion energy vs spin density) is shown in Figure S5 with the dispersion energies calculated at these new geometries. Although some differences are observed, they are qualitatively similar.

EXPERIMENTAL METHODS

Oxidation to Generate Radicals. The C−H aryl malononitrile precursors were oxidized to form the radical/dimers using previously reported methods.[31,33] For radicals **1**−**5** and **9**−**10**, a biphasic oxidation between basic aqueous potassium ferricyanate and dichloro-

https://dx.doi.org/10.1021/jacs.0c00190
J. Am. Chem. Soc. 2020, 142, 5304−5313

methane was used. For all other radicals, **6**−**8** and **11**−**14**, the aryl malononitrile was dissolved in the solvent of study, then lead(IV) oxide was added in excess, and the resulting mixture was mixed for 5−10 min. After removal of all excess solids by centrifugation, quantitative oxidation to radicals was indicated by absence of starting material peaks in the ^{1}H NMR spectrum.

Association Constants and van 't Hoff Plots. The dimerization thermodynamic parameters for each of the radicals was determined by variable temperature EPR. From the double integration of each EPR spectra, equilibrium constants were obtained. Intermolecular binding constants were calculated from a van 't Hoff plot. An example is shown in Table 1, and all plots are included in the Supporting Information. The EPR instrument was calibrated with a TEMPO standard. A van't Hoff plot ($\ln K_{eq}$ vs $1/T$) provides the equilibrium parameters ($\Delta H°$ and $\Delta S°$, which lead to $\Delta G°$ and K_a values) for each system. It is important to note that EPR spectroscopy is blind to the nature of spin-paired species (σ-dimer or pimer) so the K_a value is really measuring the equilibrium between EPR-inactive diamagnetic dimers and spin-unpaired free radicals (or possibly thermally populated triplet excited states of the pimers, at high temperatures).

Determining Mode of Radical Dimerization and Low Temperature UV−Vis Measurements. In general, the mode of dimerization for each radical was determined by change in color of the solutions. For σ-dimers, the solution turns clear or yellow upon cooling in a dry ice/acetone bath, while for pimers the solutions turns darker blue. These results were also observable using a UV−vis spectrometer with low-temperature capability. All UV−vis experiments started with a known concentration of radical prepared by oxidation of the malononitrile derivative. A UV−vis spectrometer with liquid nitrogen cooling capabilities was used under inert atmosphere to avoid water vapor condensation. A temperature curve calibration was used to determine accurate temperature measurements at various data points. Sampling intervals were performed at 0.2 nm increments and equilibration of temperature was allowed for 5 min prior to each spectrum being acquired. Because both the σ-dimer and pimer are in equilibrium, observation of a pimer does not rule out the possibility of a low-energy or near degenerate σ-dimer that may also be present in the equilibrium at higher temperatures. In some cases, pimers were observed at higher concentrations but not low concentrations, suggesting in these cases that, while the σ-dimer is likely the lower energy form, the pimer is close enough in energy to be thermally populated, which can be observed at higher concentrations, and suggesting these dimeric forms are nearly degenerate. We listed these in the graphs as "pimer observed", although the near-degeneracy of the two dimers is likely, and the σ-dimer form may even be the lower energy form.

EPR Measurements and Parameters. After oxidation of each radical precursor to generate the radical, solutions of each radical were purged and placed under an inert atmosphere to remove oxygen. Solutions of toluene allowed the use of a 3 mm quartz EPR tube. When performing variable temperature EPR analysis, solutions were allowed to equilibrate at each temperature for 5 min before each scan. Every data point is an average of a minimum of eight scans, with more scans used in cases where small radical signals were observed. The following instrument parameters were utilized for all compounds at all temperatures: modulation frequency, 100 kHz; receiver gain, 50 dB; modulation amplitude, 0.5 G; time constant, 0.01 s; center field, 3335 G; sweep width, 150 G; microwave attenuation, 20 dB; microwave power, 2 mW; number of data points, 2048.

CONCLUSIONS

In conclusion, we have demonstrated that the mode of dimerization of dicyanomethyl radicals can be reasonably predicted by two parameter models using computational predictions of spin density delocalization or the radical polarizability and computational estimates of the π-dimer dispersion stabilization energy. The importance of polarization can be seen by the change in the charge densities upon pimerization, and the preferred geometry of the pimer as a head-to-tail dimer, while the head-to-head pimer is not even a minimum on the potential energy surface. Care was taken to isolate electronic effects by choosing neutral radicals that are planar and not sterically hindered at the radical center. This can be viewed as both a strength and a weakness of this study. The strength is that electronic effects can be more clearly elucidated. A weakness of this study, then, is that steric effects or charge repulsion effects that could be important for radicals that are not planar, have bulky groups attached, or are charged, are not considered here. For example, a radical that forms a σ-dimer might prefer to form a pimer if bulky substituents are attached adjacent to the radical center (see Figure 1 for an example of this with the phenallenyl radical).

We find that for radicals with greater than 45% spin density on the benzylic dicyanomethyl carbon, only σ-dimerization is observed. Such highly localized spins correlates to radical/dimer binding constants of 10^5 M^{-1} or greater. In contrast, with more delocalized radicals (<45% spin density on the benzylic carbon), either σ-dimerization or pimerization can occur, with radicals with strong pimer dispersion energies forming pimers while those with weak dispersion interactions forming σ-dimers. While we have yet to identify a computational method that can accurately predict the radical−σ-dimer−pimer thermodynamics for these radicals, simple models that can explain and predict the interactions of such radicals, such as the ones developed in this paper, may prove to be useful for explaining and predicting the properties of new radicals. Importantly, this work suggests that both radical delocalization, polarization, and dispersion forces are important in dictating the mode of dimerization for metastable radicals, and provides a theoretical framework for explaining the behavior of known radicals and predicting the behavior of novel radicals.

At present, some humility in our ability to conceptually understand the features that lead to small changes in relative energy is needed. For a few of the radicals in our library, at low concentrations of the radical we observe visually the σ-dimer at low temperature, as indicated by the colored solutions of radical turning clear or yellow as the temperature is lowered. Yet, at much higher concentrations, the solutions turn darker blue upon cooling, the hallmark indicator for the formation of the pimer. This observation suggests that, for these radicals, the σ-dimer and pimer forms are nearly degenerate. Most likely, at low temperatures, there is still a thermal population of the higher-energy pimer form that can only be observed visually at high concentrations. In this regime, where the two radical dimeric forms may be separated by less than 1 kcal/mol in free energy, the subtle features that lead to a small change in the relative stability of the σ-dimer/pimer may not be perfectly captured by relatively crude indices such as "polarizability," "spin delocalization," and "dispersion" that relate mostly to enthalpy and ignore entropy.

Furthermore, models can be useful and predictive without being built on any bedrock truth. Therefore, the imperfect but somewhat surprising success of the two-parameter models described here does not necessarily mean that the parameters themselves are important directing features. They may be merely indicators. Nevertheless, it is tempting to interpret the clear correlation and predictive power of the computed spin density on the benzylic carbon with the experimentally determined K_a values (Figure 6, top) as demonstrating the importance of spin (de)localization on the stability of the free radical relative to either dimeric form. Less clear are the

https://dx.doi.org/10.1021/jacs.0c00190
J. Am. Chem. Soc. 2020, 142, 5304−5313

importance of polarizability and dispersion forces, although none of our models are successful without including pimer dispersion estimates, and the polarizability hypothesis explains nicely why the pimer adopts the head-to-tail structure and why the head-to-head pimer does not appear to be a local minimum. Subject to the usual caveats about models and reality, it is reasonable to suggest that (at least) these three effects are important in governing the formation of diradical pimers.

■ ASSOCIATED CONTENT

Supporting Information

The Supporting Information is available free of charge at https://pubs.acs.org/doi/10.1021/jacs.0c00190.

Crystallographic data for **7** σ-dimer (CIF)

Crystallographic data for **9** σ-dimer (CIF)

Crystallographic data for **4** σ-dimer (CIF)

Computational synthetic procedures, Cartesian coordinates, UV−vis spectra, van 't Hoff plots (PDF)

■ AUTHOR INFORMATION

Corresponding Author

Arthur H. Winter − *Department of Chemistry, Iowa State University, Ames, Iowa 50010, United States;* orcid.org/0000-0003-2421-5578; Email: winter@iastate.edu

Authors

Joshua P. Peterson − *Department of Chemistry, Iowa State University, Ames, Iowa 50010, United States;* orcid.org/0000-0002-9897-238X

Arkady Ellern − *Department of Chemistry, Iowa State University, Ames, Iowa 50010, United States*

Complete contact information is available at: https://pubs.acs.org/10.1021/jacs.0c00190

Notes

The authors declare no competing financial interest.

■ ACKNOWLEDGMENTS

We thank the Iowa State Chemical Instrumentation Facility, specifically Dr. Sarah Cady, for EPR guidance. We thank the National Science Foundation (NSF) (CHE-1464956) and the Bailey Research Award for financial support. We also thank HPC@ISU for equipment use at Iowa State University, some of which was purchased through funding provided by the NSF under MRI Grant CBS 1229081 and CRI Grant1205413.

■ REFERENCES

(1) Gomberg, M. An Instance of Trivalent Carbon: Triphenylmethyl. *J. Am. Chem. Soc.* **1900**, *22* (11), 757−771.

(2) Grossel, M. C.; Weston, S. C. Synthesis of materials for molecular electronic applications. *Contemp. Org. Synth.* **1994**, *1* (5), 367−386.

(3) Hughes, B. K.; Braunecker, W. A.; Bobela, D. C.; Nanayakkara, S. U.; Reid, O. G.; Johnson, J. C. Covalently Bound Nitroxyl Radicals in an Organic Framework. *J. Phys. Chem. Lett.* **2016**, *7* (18), 3660−5.

(4) Li, L. H.; Feng, X. L.; Cui, X. H.; Ma, Y. X.; Ding, S. Y.; Wang, W. Salen-Based Covalent Organic Framework. *J. Am. Chem. Soc.* **2017**, *139* (17), 6042−6045.

(5) Juetten, M. J.; Buck, A. T.; Winter, A. H. A radical spin on viologen polymers: organic spin crossover materials in water. *Chem. Commun. (Cambridge, U. K.)* **2015**, *51* (25), 5516−9.

(6) Rajca, A. Organic Diradicals and Polyradicals: From Spin Coupling to Magnetism? *Chem. Rev.* **1994**, *94* (4), 871−893.

(7) Rowan, S. J.; Cantrill, S. J.; Cousins, G. R. L.; Sanders, J. K. M.; Stoddart, J. F. Dynamic Covalent Chemistry. *Angew. Chem., Int. Ed.* **2002**, *41* (6), 898−952.

(8) Jin, Y.; Yu, C.; Denman, R. J.; Zhang, W. Recent advances in dynamic covalent chemistry. *Chem. Soc. Rev.* **2013**, *42* (16), 6634−6654.

(9) Morita, Y.; Suzuki, S.; Sato, K.; Takui, T. Synthetic organic spin chemistry for structurally well-defined open-shell graphene fragments. *Nat. Chem.* **2011**, *3* (3), 197−204.

(10) Rajca, A.; Wang, Y.; Boska, M.; Paletta, J. T.; Olankitwanit, A.; Swanson, M. A.; Mitchell, D. G.; Eaton, S. S.; Eaton, G. R.; Rajca, S. Organic Radical Contrast Agents for Magnetic Resonance Imaging. *J. Am. Chem. Soc.* **2012**, *134* (38), 15724−15727.

(11) Kobayashi, H.; Danno, T.; Saito, Y. The Crystal structure of bis(trimethylammonium) tris(7,7,8,8-tetracyanoquinodimethanide), $(TMA^{+})_2$ $(TCNQ)_3^{2-}$. *Acta Crystallogr., Sect. B: Struct. Crystallogr. Cryst. Chem.* **1973**, *29* (12), 2693−2699.

(12) Penneau, J. F.; Stallman, B. J.; Kasai, P. H.; Miller, L. L. An imide anion radical that dimerizes and assembles into.pi.-stacks in solution. *Chem. Mater.* **1991**, *3* (5), 791−796.

(13) Rösel, S.; Becker, J.; Allen, W. D.; Schreiner, P. R. Probing the Delicate Balance between Pauli Repulsion and London Dispersion with Triphenylmethyl Derivatives. *J. Am. Chem. Soc.* **2018**, *140* (43), 14421−14432.

(14) Rösel, S.; Balestrieri, C.; Schreiner, P. R. Sizing the role of London dispersion in the dissociation of all-meta tert-butyl hexaphenylethane. *Chemical Science* **2017**, *8* (1), 405−410.

(15) Lekin, K.; Phan, H.; Winter, S. M.; Wong, J. W. L.; Leitch, A. A.; Laniel, D.; Yong, W.; Secco, R. A.; Tse, J. S.; Desgreniers, S.; Dube, P. A.; Shatruk, M.; Oakley, R. T. Heat, Pressure and Light-Induced Interconversion of Bisdithiazolyl Radicals and Dimers. *J. Am. Chem. Soc.* **2014**, *136* (22), 8050−8062.

(16) Yokoi, H.; Hiroto, S.; Shinokubo, H. Reversible σ-Bond Formation in Bowl-Shaped π-Radical Cations: The Effects of Curved and Planar Structures. *J. Am. Chem. Soc.* **2018**, *140* (13), 4649−4655.

(17) Dragulescu-Andrasi, A.; Filatov, A. S.; Oakley, R. T.; Li, X.; Lekin, K.; Huq, A.; Pak, C.; Greer, S. M.; McKay, J.; Jo, M.; Lengyel, J.; Hung, I.; Maradzike, E.; DePrince, A. E.; Stoian, S. A.; Hill, S.; Hu, Y.-Y.; Shatruk, M. Radical Dimerization in a Plastic Organic Crystal Leads to Structural and Magnetic Bistability with Wide Thermal Hysteresis. *J. Am. Chem. Soc.* **2019**, *141*, 17989.

(18) Geraskina, M. R.; Dutton, A. S.; Juetten, M. J.; Wood, S. A.; Winter, A. H. The Viologen Cation Radical Pimer: A Case of Dispersion-Driven Bonding. *Angew. Chem., Int. Ed.* **2017**, *56* (32), 9435−9439.

(19) Constantinides, C. P.; Carter, E.; Eisler, D.; Beldjoudi, Y.; Murphy, D. M.; Rawson, J. M. Effects of Halo-Substitution on 2'-Chloro-5′-halo-phenyl-1,2,3,5-dithiadiazolyl Radicals: A Crystallographic, Magnetic, and Electron Paramagnetic Resonance Case Study. *Cryst. Growth Des.* **2017**, *17* (6), 3017−3029.

(20) Mou, Z.; Kertesz, M. Sigma- versus Pi-Dimerization Modes of Triangulene. *Chem. - Eur. J.* **2018**, *24* (23), 6140−6147.

(21) Kertesz, M. Pancake Bonding: An Unusual Pi-Stacking Interaction. *Chem. - Eur. J.* **2019**, *25* (2), 400−416.

(22) Pal, S. K.; Itkis, M. E.; Tham, F. S.; Reed, R. W.; Oakley, R. T.; Haddon, R. C. Resonating Valence-Bond Ground State in a Phenalenyl-Based Neutral Radical Conductor. *Science* **2005**, *309* (5732), 281.

(23) Fujita, W.; Awaga, a. K. Room-Temperature Magnetic Bistability in Organic Radical Crystals. *Science* **1999**, *286* (5438), 261.

(24) Mou, Z.; Kubo, T.; Kertesz, M. Hetero-π-Dimers of Phenalenyls. *Chem. - Eur. J.* **2015**, *21* (50), 18230−18236.

(25) Mou, Z.; Uchida, K.; Kubo, T.; Kertesz, M. Evidence of σ- and π-Dimerization in a Series of Phenalenyls. *J. Am. Chem. Soc.* **2014**, *136* (52), 18009−18022.

(26) Uchida, K.; Mou, Z.; Kertesz, M.; Kubo, T. Fluxional σ-Bonds of the 2,5,8-Trimethylphenalenyl Dimer: Direct Observation of the

Sixfold σ-Bond Shift via a π-Dimer. *J. Am. Chem. Soc.* **2016**, *138* (13), 4665−4672.
(27) Kosower, E. M.; Poziomek, E. J. Stable Free Radicals. I. Isolation and Distillation of 1-Ethyl-4-carbomethoxypyridinyl. *J. Am. Chem. Soc.* **1964**, *86* (24), 5515−5523.
(28) Itkis, M. E.; Chi, X.; Cordes, A. W.; Haddon, R. C. Magneto-Opto-Electronic Bistability in a Phenalenyl-Based Neutral Radical. *Science* **2002**, *296* (5572), 1443.
(29) Koivisto, B. D.; Ichimura, A. S.; McDonald, R.; Lemaire, M. T.; Thompson, L. K.; Hicks, R. G. Intramolecular π-Dimerization in a 1,1′-Bis(verdazyl)ferrocene Diradical. *J. Am. Chem. Soc.* **2006**, *128* (3), 690−691.
(30) Melen, R. L.; Less, R. J.; Pask, C. M.; Rawson, J. M. Structural Studies of Perfluoroaryldiselenadiazolyl Radicals: Insights into Dithiadiazolyl Chemistry. *Inorg. Chem.* **2016**, *55* (22), 11747−11759.
(31) Peterson, J. P.; Geraskina, M. R.; Zhang, R.; Winter, A. H. Effect of Substituents on the Bond Strength of Air-Stable Dicyanomethyl Radical Thermochromes. *J. Org. Chem.* **2017**, *82* (12), 6497−6501.
(32) Okino, K.; Hira, S.; Inoue, Y.; Sakamaki, D.; Seki, S. The Divergent Dimerization Behavior of N-Substituted Dicyanomethyl Radicals: Dynamically Stabilized versus Stable Radicals. *Angew. Chem.* **2017**, *129* (52), 16824−16828.
(33) Kobashi, T.; Sakamaki, D.; Seki, S. N-Substituted Dicyanomethylphenyl Radicals: Dynamic Covalent Properties and Formation of Stimuli-Responsive Cyclophanes by Self-Assembly. *Angew. Chem., Int. Ed.* **2016**, *55* (30), 8634−8638.
(34) Okino, K.; Sakamaki, D.; Seki, S. Dicyanomethyl Radical-Based Near-Infrared Thermochromic Dyes with High Transparency in the Visible Region. *ACS Materials Letters* **2019**, *1*, 25−29.
(35) Peterson, J. P.; Zhang, R.; Winter, A. H. Effect of Structure on the Spin Switching and Magnetic Bistability of Solid-State Aryl Dicyanomethyl Monoradicals and Diradicals. *ACS Omega* **2019**, *4*, 13538.
(36) Peterson, J. P.; Winter, A. H. Solvent Effects on the Stability and Delocalization of Aryl Dicyanomethyl Radicals: The Captodative Effect Revisited. *J. Am. Chem. Soc.* **2019**, *141*, 12901.
(37) Zhang, R.; Peterson, J. P.; Fischer, L. J.; Ellern, A.; Winter, A. H. Effect of Structure on the Spin−Spin Interactions of Tethered Dicyanomethyl Diradicals. *J. Am. Chem. Soc.* **2018**, *140*, 14308.
(38) Alabugin, I. V. *Stereoelectronic Effects: A Bridge Between Structure and Reactivity*; Wiley: 2016.
(39) Syroeshkin, M. A.; Kuriakose, F.; Saverina, E. A.; Timofeeva, V. A.; Egorov, M. P.; Alabugin, I. V. Upconversion of Reductants. *Angew. Chem., Int. Ed.* **2019**, *58* (17), 5532−5550.
(40) Awere, E. G.; Burford, N.; Haddon, R. C.; Parsons, S.; Passmore, J.; Waszczak, J. V.; White, P. S. X-ray crystal structures of the 1,3,2-benzodithiazolyl dimer and 1,3,2-benzodithiazolium chloride sulfur dioxide solvate: comparison of the molecular and electronic structures of the 10-.pi.-electron C6H4S2N+ cation and the C6H4S2N.bul. radical and dimer and a study of the variable-temperature magnetic behavior of the radical. *Inorg. Chem.* **1990**, *29* (23), 4821−4830.
(41) Ould, D. M. C.; Tran, T. T. P.; Rawson, J. M.; Melen, R. L. Structure−property-reactivity studies on dithiaphospholes. *Dalton Transactions* **2019**, *48* (45), 16922−16935.
(42) Knizia, G. Intrinsic Atomic Orbitals: An Unbiased Bridge between Quantum Theory and Chemical Concepts. *J. Chem. Theory Comput.* **2013**, *9* (11), 4834−4843.
(43) Knizia, G.; Klein, J. E. M. N. Electron Flow in Reaction Mechanisms—Revealed from First Principles. *Angew. Chem., Int. Ed.* **2015**, *54* (18), 5518−5522.
(44) Chai, J.-D.; Head-Gordon, M. Long-range corrected hybrid density functionals with damped atom−atom dispersion corrections. *Phys. Chem. Chem. Phys.* **2008**, *10* (44), 6615−6620.
(45) Frisch, M. J.; Trucks, G. W.; Schlegel, H. B.; Scuseria, G. E.; Robb, M. A.; Cheeseman, J. R.; Scalmani, G.; Barone, V.; Petersson, G. A.; Nakatsuji, H.; Li, X.; Caricato, M.; Marenich, A. V.; Bloino, J.; Janesko, B. G.; Gomperts, R.; Mennucci, B.; Hratchian, H. P.; Ortiz, J. V.; Izmaylov, A. F.; Sonnenberg, J. L.; Williams; Ding, F.; Lipparini, F.; Egidi, F.; Goings, J.; Peng, B.; Petrone, A.; Henderson, T.; Ranasinghe, D.; Zakrzewski, V. G.; Gao, J.; Rega, N.; Zheng, G.; Liang, W.; Hada, M.; Ehara, M.; Toyota, K.; Fukuda, R.; Hasegawa, J.; Ishida, M.; Nakajima, T.; Honda, Y.; Kitao, O.; Nakai, H.; Vreven, T.; Throssell, K.; Montgomery, J. A., Jr.; Peralta, J. E.; Ogliaro, F.; Bearpark, M. J.; Heyd, J. J.; Brothers, E. N.; Kudin, K. N.; Staroverov, V. N.; Keith, T. A.; Kobayashi, R.; Normand, J.; Raghavachari, K.; Rendell, A. P.; Burant, J. C.; Iyengar, S. S.; Tomasi, J.; Cossi, M.; Millam, J. M.; Klene, M.; Adamo, C.; Cammi, R.; Ochterski, J. W.; Martin, R. L.; Morokuma, K.; Farkas, O.; Foresman, J. B.; Fox, D. J. *Gaussian 16*, Rev. C.01; Gaussian Inc.: Wallingford, CT, 2016.
(46) Grimme, S. Semiempirical GGA-type density functional constructed with a long-range dispersion correction. *J. Comput. Chem.* **2006**, *27* (15), 1787−1799.
(47) Schmider, H. L.; Becke, A. D. Optimized density functionals from the extended G2 test set. *J. Chem. Phys.* **1998**, *108* (23), 9624−9631.

https://dx.doi.org/10.1021/jacs.0c00190
J. Am. Chem. Soc. 2020, 142, 5304−5313